1B.3 TURBULENCE STRUCTURE AND MIXING IN STRONGLY STABLE BOUNDARY-LAYER FLOWS OVER THERMALLY HETEROGENEOUS SURFACES

Dmitrii Mironov[1]* and Peter Sullivan[2]

[1] German Weather Service, Offenbach am Main, Germany
[2] National Center for Atmospheric Research, Boulder, CO, USA

1. INTRODUCTION

Representation of stably stratified planetary boundary layer (SBL) presents a serious problem for numerical weather prediction, climate modeling, and related applications. Model errors associated with the SBL regimes characterized by relatively weak turbulence and low mixing intensity are often substantial, and it is still largely unclear how the trouble can be cured. Many SBL features are poorly understood (see, e.g., Mahrt, 2014, for discussion). One particularly challenging issue is the strongly stable boundary layer over a thermally heterogeneous surface. In the present study, we use direct numerical simulation (DNS) to gain some insight into the effect of surface thermal heterogeneity on the structure and transport properties of strongly stable boundary layer.

Mironov and Sullivan (2016, hereafter MS16) used large-eddy simulation (LES) to examine the mean and turbulence structure of the atmospheric SBL over thermally homogeneous and thermally heterogeneous surfaces. The LES data were used to perform a comparative analysis of second-moment budgets and mixing intensity in the homogeneous and heterogeneous SBLs. A physically plausible explanation of the enhanced mixing in the heterogeneous SBL was found, and possible ways to parameterize the heterogeneity effects in atmospheric models were discussed. It should be emphasized that the results of MS16 are pertinent to weakly-to-moderately stable boundary layers characterized by continuous and rather vigorous turbulence. The structure and mixing intensity in strongly stable boundary layers characterized by weak and often intermittent turbulence are still largely unknown and need to be investigated. The present study attempts to make a step forward in this direction.

Among other questions, the following outstanding questions should be addressed. (i) If turbulence dies out over a homogeneous surface due to strong stability, does it survive over a heterogeneous surface? (ii) If turbulence survives, how anisotropic does it appear to be and does it generate appreciable vertical fluxes of momentum and scalars? (iii) What are the particular features of the second-moment budgets in strongly stable regime, and what is the role of the pressure-scrambling and of the third-order transport in maintaining the variance and flux budgets? The present contribution addresses the issues (i) and (ii). Analysis of the second-moment budgets is left for future studies.

The present study is not aimed at simulating the real-world geophysical (e.g., atmospheric or oceanic) flows. Instead, we focus on physical processes at work in strongly stratified boundary-layer flows, namely, on the effect of surface thermal heterogeneity on the structure and transport properties of turbulence. To this end, we use an idealized plane Couette flow set-up (a physical analogue of our numerical configuration is discussed in the next section). The flow is driven by a fixed velocity of the upper surface, while the lower surface is at rest. The stable density stratification is imposed by a fixed temperature difference between the upper and lower boundaries. The temperature at the horizontal upper and lower surfaces is either homogeneous or varies sinusoidally in the streamwise direction, while the horizontal-mean temperature is the same in the homogeneous and heterogeneous cases. The DNS data are used to compute the vertical profiles of mean fields and of the second-order and (some) third-order statistical moments of turbulence, and to analyze the structure and mixing intensity of the flows over thermally homogeneous and thermally heterogeneous surfaces.

The plane Couette flow configuration has often been used to study various aspects of neutral, convective and stably stratified turbulence (see, e.g., Komminaho et al., 1996; Papavassiliou and Hanratty, 1997; Sullivan et al., 2000; Sullivan and McWilliams, 2002; Avsarkisov et al., 2014; Richter and Sullivan, 2014; Deusebio et al., 2015, and references therein). To the best of the authors' knowledge, DNS of Couette flows over thermally heterogeneous surfaces has not been performed so far.

The flow configuration and governing equations are described in section 2. Details of the simulations performed are given in section 3. Simulation results are discussed in section 4. Conclusions are presented in section 5.

---

[*] *Corresponding author address:* Dmitrii Mironov, Deutscher Wetterdienst, FE14, Frankfurter Str. 135, D-63067 Offenbach am Main, Germany; *e-mail*: dmitrii.mironov@dwd.de

2. FLOW CONFIGURATION AND GOVERNING EQUATIONS

We consider a three-dimensional, stably stratified, plane Couette flow. The fluid depth is H, the lower boundary is at rest, and the upper boundary moves with a constant velocity U_u. Stable buoyancy stratification is maintained by a temperature difference $\Delta\theta = \theta_u - \theta_l$ between the upper and lower boundaries. The physical characteristics of the fluid are the kinematic molecular viscosity ν, the molecular temperature conductivity κ, and the buoyancy parameter $\beta_i = -g_i \alpha_T$, where g_i is the acceleration due to gravity and α_T is the thermal expansion coefficient. Both ν and κ are taken to be constant in our simulations. The Boussinesq approximation is used, and the simplest linear equation of state is utilized, $\rho = \rho_r [1 - \alpha_T (\theta - \theta_r)]$, where ρ is the fluid density, ρ_r is the constant reference density, θ is the potential temperature (for the sake of brevity, it will also be referred to as simply "temperature"), and θ_r is the constant reference potential temperature. Both α_T and β_i are constant.

The governing equations given below contain three dimensionless parameters. These are the Reynolds number,

$$\mathrm{Re} = \frac{U_u H}{\nu}, \tag{1}$$

the Prandtl number,

$$\mathrm{Pr} = \frac{\nu}{\kappa}, \tag{2}$$

and the Richardson number,

$$\mathrm{Ri} = \frac{g_3 H \alpha_T \Delta\theta}{U_u^2}, \tag{3}$$

where g_3 is the magnitude of the vector of gravity [in the co-ordinate system used here, $g_i = (0, 0, -g_3)$].

A real-world flow configuration closely analogous to our numerical configuration can hardly be found among geophysical flows. A conceivable physical analogue of our numerical set-up is a laboratory tank filled with the fresh water at room temperature. Using $H = 0.25$ m, $U_u = 0.04$ m s^{-1} and $\nu = 10^{-6}$ m^2 s^{-1} (the value for fresh water at 20°C), we obtain $\mathrm{Re} = 10^4$. Using a quadratic fresh-water equation of state (Mironov et al., 2010), $\rho = \rho_r \left[1 - \frac{1}{2} a_T (\theta - \theta_r)^2\right]$, where $a_T = 1.6509 \times 10^{-5}$ K^{-2} is an empirical coefficient and $\theta_r = 277.13$ K is the temperature of maximum density of fresh water, we find that a temperature difference between the upper and lover horizontal boundaries of about 1 K is needed to obtain $\mathrm{Ri} = 0.5$. To arrive at this estimate, we recast the Richardson number in terms of buoyancy difference between the upper and lover horizontal boundaries, $\mathrm{Ri} = H\Delta b / U_u^2$, where $b = g_3 (\rho_r - \rho)/\rho_r$, and use $g_3 = 9.81$ m s^{-1}, $\theta_l = 292.65$ K (19.5°C), and $\theta_u = 293.65$ K (20.5°C). Note that the Prandtl number is about 7 for fresh water (at 20°C), which is considerably higher than the value of $\mathrm{Pr} = 1$ that we adopt for our numerical fluid.

The flow variables are made dimensionless with the length scale H, velocity scale U_u, time scale H/U_u and temperature scale $\Delta\theta$, and dimensionless temperature $\hat{\theta} = (\theta - \theta_l)/(\theta_u - \theta_l)$ is introduced. The governing equations written in dimensionless form are (in order to simplify the notation, we omit hats over dimensionless variables)

$$\left(\frac{\partial}{\partial t} + u_k \frac{\partial}{\partial x_k}\right) u_i = -\frac{\partial p}{\partial x_i} + \delta_{i3} \mathrm{Ri}\,\theta + \frac{1}{\mathrm{Re}} \frac{\partial^2 u_i}{\partial x_k^2}, \tag{4}$$

$$\frac{\partial u_i}{\partial x_i} = 0, \tag{5}$$

$$\left(\frac{\partial}{\partial t} + u_i \frac{\partial}{\partial x_i}\right) \theta = \frac{1}{\mathrm{PrRe}} \frac{\partial^2 \theta}{\partial x_i^2}. \tag{6}$$

Here, t is time, x_i are the right-hand Cartesian co-ordinates, u_i are the velocity components, and p is the kinematic pressure (deviation of pressure from the hydrostatically balanced reference pressure divided by the constant reference density). The Einstein summation convention for repeated indices is adopted. The origin of the co-ordinate system is at the lower boundary, the x_3 axis is aligned with the vector of gravity and is positive upward, and the x_1 axis is in the direction of U_u. Note that, since the vertical-velocity equation in our simulations is solved for the fluctuation of u_3 about its horizontal mean, θ_r can be set equal to θ_l so that the dimensionless reference temperature $(\theta_r - \theta_l)/(\theta_u - \theta_l)$ drops out from the buoyancy term on the right-hand side (r.h.s.) of Eq. (4).

Periodic boundary conditions for u_i and θ are applied in both x_1 and x_2 horizontal directions. At the horizontal boundaries, the following Dirichlet boundary conditions are used:

$$\begin{array}{llll} u_1 = 0, & u_2 = u_3 = 0 & \text{at} & x_3 = 0, \\ u_1 = 1, & u_2 = u_3 = 0 & \text{at} & x_3 = 1, \end{array} \tag{7}$$

and

$$\begin{array}{lll} \theta = \delta\theta \sin\left[2\pi n x_1 / L_1\right] & \text{at} & x_3 = 0, \\ \theta = 1 + \delta\theta \sin\left[2\pi n (x_1 - U_u t)/L_1\right] & \text{at} & x_3 = 1, \end{array} \tag{8}$$

where L_1 is the domain size in the x_1 direction, $\delta\theta$ is the (dimensionless) amplitude of the temperature variations at the upper and lower surfaces, and n is the number of cold and warm stripes (the number of surface temperature waves). In the homogeneous case, $\delta\theta = 0$. In the heterogeneous cases, $\delta\theta > 0$ but the horizontal-mean surface temperature is the same as in the homogeneous case.

3. SIMULATIONS PERFORMED

The DNS code used in the present study is described in detail in Sullivan et al. (2000) and Sullivan and McWilliams (2002). A description of the code is not repeated here; readers are referred to the above papers.

One simulation with homogeneous lower and upper surfaces (HOM) and three simulations with heterogeneous surfaces (HET) are performed. In all simulated cases, the fixed values of $\mathrm{Pr}=1$, $\mathrm{Re}=10^4$, and $\mathrm{Ri}=0.25$ are used. The number of grid points is 512, 512, and 256 the streamwise x_1, spanwise x_2, and vertical x_3 directions, respectively. The domain size in the vertical direction is 1, and the domain size in both horizontal directions is 8. The number of cold and warm stripes (the number of surface temperature waves) in the heterogeneous cases is 4. Governing parameters of the simulations performed are summarized in Table 1.

Table 1: Governing parameters of simulated cases.

Case	$\delta\theta$	T_t	T_s	Re_τ	$Q_* \times 10^5$
HOM	0.00	715	15	104.63	-10.0
HET025	0.25	1166	166	100.50	-9.80
HET050	0.50	1392	392	107.77	-7.45
HET075	0.75	1380	380	112.16	-5.12

In Table 1, T_t is the total length of the simulation in dimensionless time units (recall that time is made dimensionless with H/U_u), T_s is the length of the sampling period (at the end of the run), $\mathrm{Re}_\tau = u_* H/\nu$ is the Reynolds number based on the surface friction velocity u_*, and Q_* is the surface temperature flux. The surface friction velocity and the two Reynolds numbers are related through $u_* = \mathrm{Re}^{-1}\mathrm{Re}_\tau$.

The homogeneous simulation starts with a fully developed, stationary, neutral Couette flow. The stable buoyancy stratification is established by gradually (linearly in time) increasing the Richardson number over 100 dimensionless time units from $\mathrm{Ri}=0$ to $\mathrm{Ri}=0.25$. The simulations are then continued until turbulence dies out and the laminar Couette flow regime is achieved. The value of $\mathrm{Ri}=0.25$ proves to be sufficient to fully quench turbulence in the homogeneous case.

The heterogeneous flows start with $\mathrm{Ri}=0$, $\delta\theta=0$, and the linear velocity profile. In order to assist initial turbulence spin-up, velocity and temperature fluctuations taken from the neutral turbulent Couette flow are added in the lower 1/4 and the upper 1/4 of the computational domain. The Richardson number is increased (linearly in time) from $\mathrm{Ri}=0$ to $\mathrm{Ri}=0.25$ over 10 time units, while the temperature difference $\delta\theta$ is increased from zero to its value given in Table 1 over 100 time units. The simulations are then continued over many time units required to achieve a quasi-stationary flow regime over heterogeneous surfaces, and then continued further in the quasi-stationary regime over the sampling period. The number of samples differs between the cases, but the sampling period in the heterogeneous cases covers more than 150 time units (see Table 1).

The DNS data are averaged over horizontal planes and the resulting profiles are then averaged over several thousand time steps. These horizontal and time mean quantities are treated as approximations to the ensemble-mean quantities. In what follows, an overbar denotes a horizontal-mean quantity, a prime denotes a fluctuation about a horizontal mean, and the angle brackets denote the quantities averaged over time.

4. RESULTS

4.1 MEAN FIELDS

Vertical profiles of the streamwise mean-velocity component $U = \langle \overline{u} \rangle$ and of mean temperature $\Theta = \langle \overline{\theta} \rangle$ are shown in Fig. 1. The spanwise mean-velocity component is negligibly small in all simulations and is not shown. In the homogeneous case, the profiles of both U and Θ are linear, corresponding to the laminar solution of the plane Couette problem. Although we give turbulence a good chance to survive by starting the homogeneous simulation with a vigorously turbulent neutral flow and gradually increasing the Richardson number, the buoyancy stratification at $\mathrm{Ri}=0.25$ is strong enough to fully extinguish turbulence.

As seen from Fig. 1, the mean velocity is only slightly affected by the surface thermal heterogeneity. The situation is different for the mean temperature. As the amplitude $\delta\theta$ of surface temperature variations increases, the flow becomes increasingly mixed with respect to Θ (the associated increase of the temperature gradient near the horizontal boundaries is due to the fact that the temperature at the boundaries is fixed). Note that the effect is appreciable at relatively large values of $\delta\theta$ in the simulations HET050 and HET075. In the simulation HET025, $\delta\theta$ is relatively small, the effect of surface heterogeneity is weak, and the temperature profile remains almost linear.

Figure 2 shows the profiles of the streamwise mean-velocity component in wall units (using the kinematic molecular viscosity and the surface friction velocity to make the profiles dimensionless), i.e., $U^+ = U\mathrm{Re}_\tau^{-1}\mathrm{Re}$ as function of $x_3^+ = x_3\mathrm{Re}_\tau$. The flow in the close vicinity of the boundaries is well resolved in our simulations. The

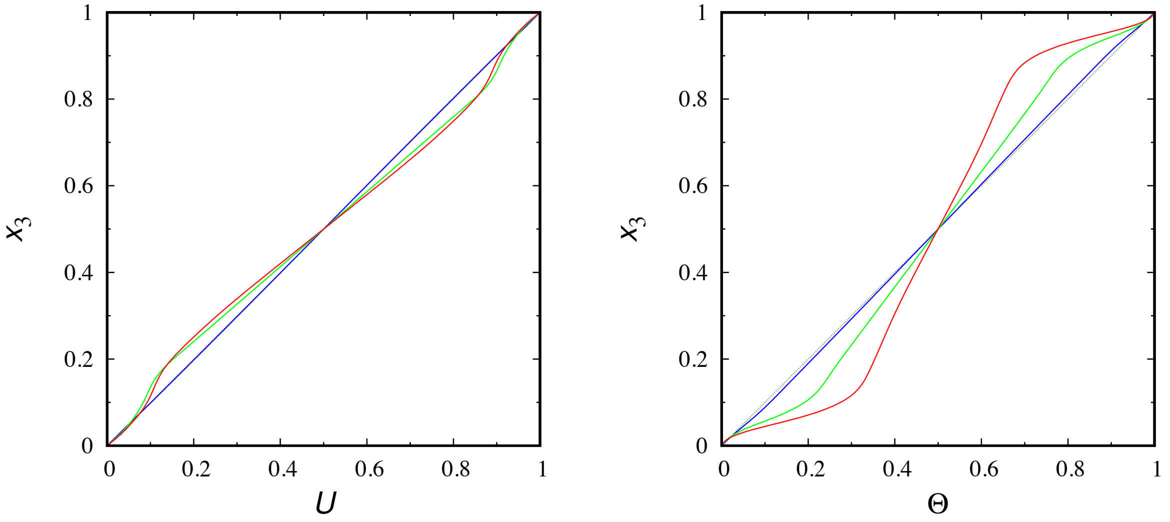

Figure 1: (left) Streamwise component of mean velocity, and (right) mean temperature from simulations HET025 (blue), HET050 (green), and HET075 (red). Thin black dotted line shows the laminar solution.

first grid point above the surface is at $x_3^+ \approx 0.2$. A larger grid spacing may be used in neutral Couette flows, but the resolution cannot be compromised in our simulations because of the need to resolve large temperature gradients in the thermal boundary layers close to the walls. It is these temperature gradients that drive turbulence in heterogeneous simulations. Test runs with lower resolution in the vertical direction yield the results (not shown) that are quantitatively and even qualitatively different from the results of high-resolution simulations and are not trustworthy. Note in passing that the domain size in horizontal directions cannot be compromised either because of the need to simulate large-scale elongated structures characteristic of plane Couette flows (e.g., Komminaho et al., 1996; Papavassiliou and Hanratty, 1997; Avsarkisov et al., 2014).

Black solid and dashed lines in Fig. 2 show, respectively, the streamwise velocity from the neutral Couette-flow simulation (the DNS data are from the run used to initialize the stably stratified HOM case) and the logarithmic velocity profile $U^+ = \frac{1}{\kappa}\ln\left(x_3^+\right) + B_0$, where $\kappa = 0.4$ and $B_0 = 5.0$ are dimensionless constants. The neural velocity profile closely follows the log-layer scaling for the height range $20 \le x_3^+ \le 200$. This is not the case for the flows over thermally heterogeneous surfaces, where the velocity profiles reveal no log-layer scaling. Green dot-dashed curve in Fig. 2 shows the Monin-Obukhov log-linear velocity profile $U^+ = \frac{1}{\kappa}\ln\left(x_3^+\right) + B_0 + \frac{C_u}{\kappa}\frac{x_3^+}{L^+}$, where $C_u = 5$ is a dimensionless constant, and $L^+ = -\left(\kappa Q_*^+ \mathrm{Re}^2 \mathrm{Ri}\right)^{-1} \mathrm{Re}_\tau^3$ and $Q_*^+ = Q_* \mathrm{Re}_\tau^{-1} \mathrm{Re}$ are, respectively, the dimensionless Obukhov length and the dimensionless surface temperature flux in wall units. The curve is computed using the governing parameters of the simulation HET050. As seen from the figure, the U^+ profile in the case HET050 (green solid curve) does not show similarity to the log-linear profile. This is not surprising, however, considering that the Monin-Obukhov surface-layer flux-profile relationships are only applicable to turbulent layers over homogeneous surfaces. For thermally heterogenous surfaces, different flux-profile relationships are required.

4.2 SECOND-ORDER MOMENTS

Figure 3 shows vertical profiles of the turbulence kinetic energy TKE$= \frac{1}{2}\left\langle \overline{u_i'^2} \right\rangle$. The TKE increases with the increasing amplitude of the surface temperature variations. The level of turbulence is very low in the case HET025, where $\delta\theta = 0.25$ proves to be too small to make the flow vigorously turbulent.

Velocity variances $uu = \left\langle \overline{u_1'^2} \right\rangle$ (streamwise), $vv = \left\langle \overline{u_2'^2} \right\rangle$ (spanwise), and $ww = \left\langle \overline{u_3'^2} \right\rangle$ (vertical) are shown in Fig. 4. In the cases HET050 and HET075, both the

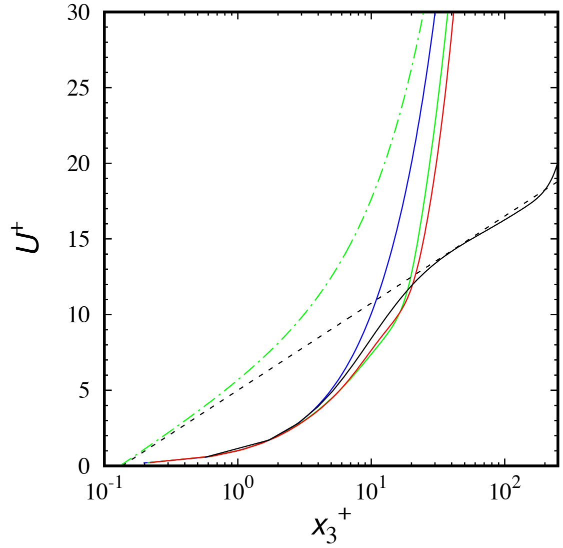

Figure 2: Streamwise mean-velocity component plotted in wall units. Solid curves snow the profiles from simulations HET025 (blue), HET050 (green), HET075 (red), and from the neutrally stratified Couette flow (black). Black dashed line shows the logarithmic velocity profile, and green dot-dashed line shows the Monin-Obukhov log-linear velocity profile computed with the surface friction velocity and the surface buoyancy flux from the simulation HET050 (see text for details).

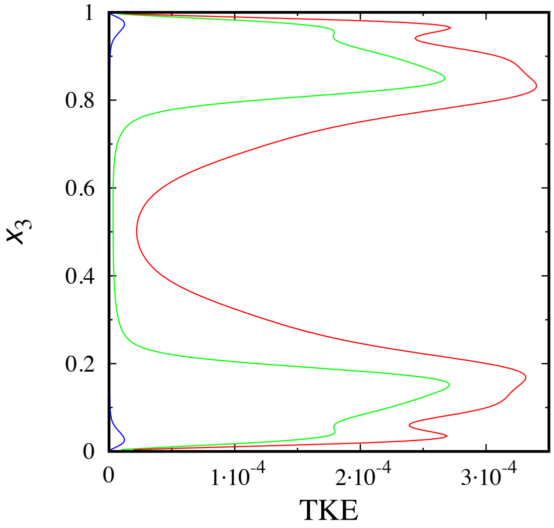

Figure 3: Turbulence kinetic energy from simulations HET025 (blue), HET050 (green), and HET075 (red).

spanwise and the vertical velocity variances are considerable, although they are a few times smaller than the streamwise velocity variance. In the case HET025, the dominating contribution to the TKE is by *uu*, whereas both *vv* and *ww* are very small.

One quantitative measure of the anisotropy of turbulence is the departure-from-isotropy tensor defined as

$$b_{ij} = \frac{\left\langle \overline{u_i' u_j'} \right\rangle}{\left\langle \overline{u_k'^2} \right\rangle} - \frac{1}{3}\delta_{ij}. \tag{9}$$

In isotropic turbulence, all components of b_{ij} are zero. In the two-component limit, where velocity fluctuations in one direction (e.g., vertical) are suppressed, the respective diagonal component of b_{ij} is equal to $-1/3$. As seen from Fig. 5, b_{33} is negative throughout the flow in the simulations HET050 and HET075, indicating that the vertical-velocity fluctuations are strongly damped by the buoyancy forces and the turbulence is strongly anisotropic. In the simulation HET025, b_{33} is positive in some regions of the flow, but turbulence there is very week and all three velocity variances, and hence the TKE, are negligibly small.

As would be expected, the temperature variance $\theta\theta = \left\langle \overline{\theta'^2} \right\rangle$, increases with the increasing amplitude of the surface temperature variations $\delta\theta$, Fig. 6. It is significant that the large values of $\theta\theta$ are confined to the immediate vicinity of the lower and upper boundaries, and the temperature variance is small in the bulk of the flow interior $0.1 \le x_3 \le 0.9$.

Vertical profiles of the streamwise momentum-flux component (denoted by *wu*) and of the vertical temperature flux (denoted by $w\theta$) are shown in Figs. 7 and 8, respectively. The spanwise momentum-flux component (not shown) is negligibly small in all simulations. In the steady state, the total fluxes, i.e., the sum of turbulent and molecular fluxes, are depth-constant. That is,

$$\left\langle \overline{u_3' u_1'} \right\rangle - \frac{1}{\mathrm{Re}} \frac{\partial \langle \overline{u_1} \rangle}{\partial x_3} = const, \tag{10}$$

and

$$\left\langle \overline{u_3' \theta'} \right\rangle - \frac{1}{\mathrm{PrRe}} \frac{\partial \langle \overline{\theta} \rangle}{\partial x_3} = const. \tag{11}$$

In the laminar Couette flow, the contributions to *wu* and $w\theta$ are due to molecular diffusion only, and the fluxes are equal to Re^{-1} and $(\mathrm{PrRe})^{-1}$, respectively.

As seen from Fig. 7, the magnitude of the total streamwise momentum-flux component increases with the increasing amplitude of the surface temperature variations. In the simulation HET025, the turbulent momentum flux is very small and the total flux is virtually the same as in the laminar flow. In the simulations HET050 and HET075, both turbulent flux and molecular flux are negative, contributing to the downward momentum transport (positive values of $\left\langle \overline{u_3' u_1'} \right\rangle$ can be identified in the case HET050, but the magnitude of positive momentum flux is negligibly small).

The total vertical temperature flux, Fig. 8, decreases with the increasing amplitude of the surface temperature variations. This is at variance with the total streamwise momentum-flux component. The total temperature flux in the simulation HET025 is very close to that in the laminar flow. However, the turbulent temperature flux $\left\langle \overline{u_3' \theta'} \right\rangle$ is not entirely negligible. A remarkable feature of the heterogeneous simulations is the sign of the vertical turbulent temperature flux. Although the flow is stably stratified in the mean sense and the total (molecular plus turbulent) vertical temperature flux is negative, the turbulent heat flux proves to be positive. Turbulent motions generated by the surface thermal heterogeneity transfer heat up the gradient of the mean temperature. It somewhat resembles convective boundary-layer flows, where quasi-organized cell-like structures cause a counter-gradient heat transport.

4.3 VERTICAL-VELOCITY AND TEMPERATURE SKEWNESS

Figure 9 shows vertical profiles of the vertical-velocity skewness $S_w = \left\langle \overline{u_3'^3} / \overline{u_3'^2}^{3/2} \right\rangle$ and of the temperature skewness $S_\theta = \left\langle \overline{\theta'^3} / \overline{\theta'^2}^{3/2} \right\rangle$. As seen from the plots, in all three heterogeneous simulations both S_w and S_θ are positive near the lower boundary. By symmetry of the flow about a horizontal plane $x_3 = 0.5$, both S_w and S_θ are negative near the upper boundary. A positive vertical-velocity skewness indicates that positive (upward) vertical velocity has a lower fractional area coverage (more localized) than negative (downward) vertical velocity. Likewise, a positive temperature skewness indicates a stronger localization of positive temperature fluctuations (about a horizontal-mean temperature) as compared to negative temperature fluctuations.

The situation is broadly similar to that in the dry convective boundary layer (CBL) driven by the surface potential-temperature (buoyancy) flux. Both S_w and S_θ are positive in the major part of the CBL, where highly localized positive potential-temperature anomalies are collocated with positive vertical velocity, forming the flow structures know as convective plumes. It is these plumes that account for most of the upward potential-temperature flux. Visualization of the u_3 and θ fields in our heterogeneous simulations (not shown)

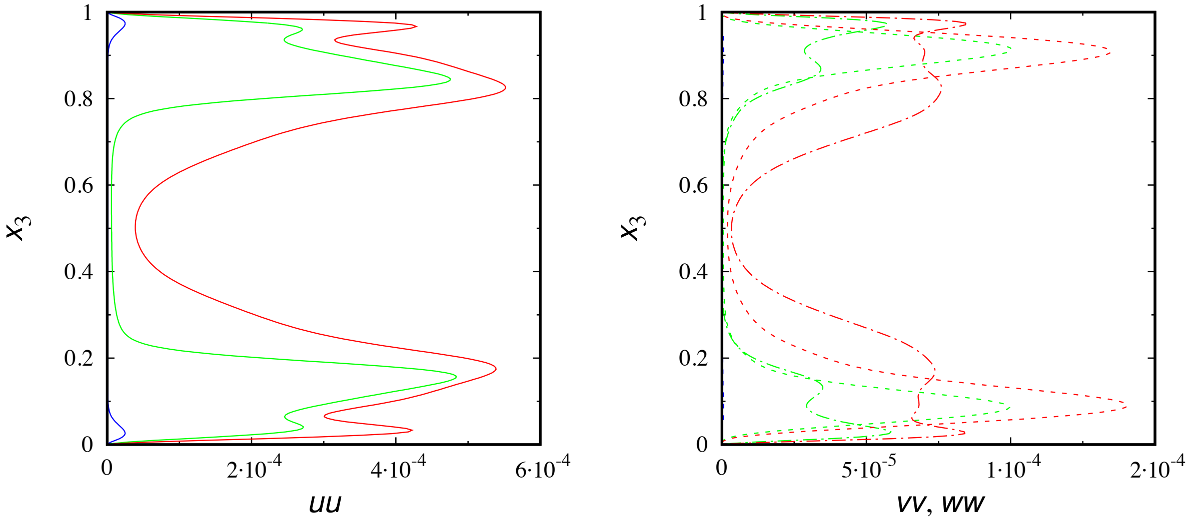

Figure 4: (left) Streamwise velocity variance, and (right) spanwise (dot-dashed curves) and vertical (dashed curves) velocity variances from simulations HET025 (blue), HET050 (green), and HET075 (red).

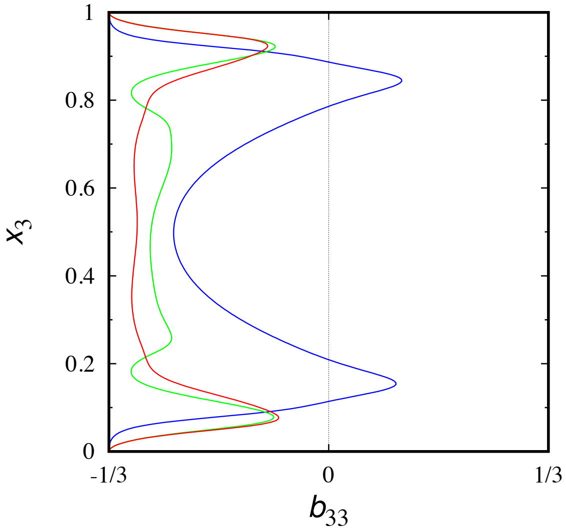

Figure 5: The b_{33} component of the departure-from-isotropy tensor, Eq. (9), from simulations HET025 (blue), HET050 (green), and HET075 (red).

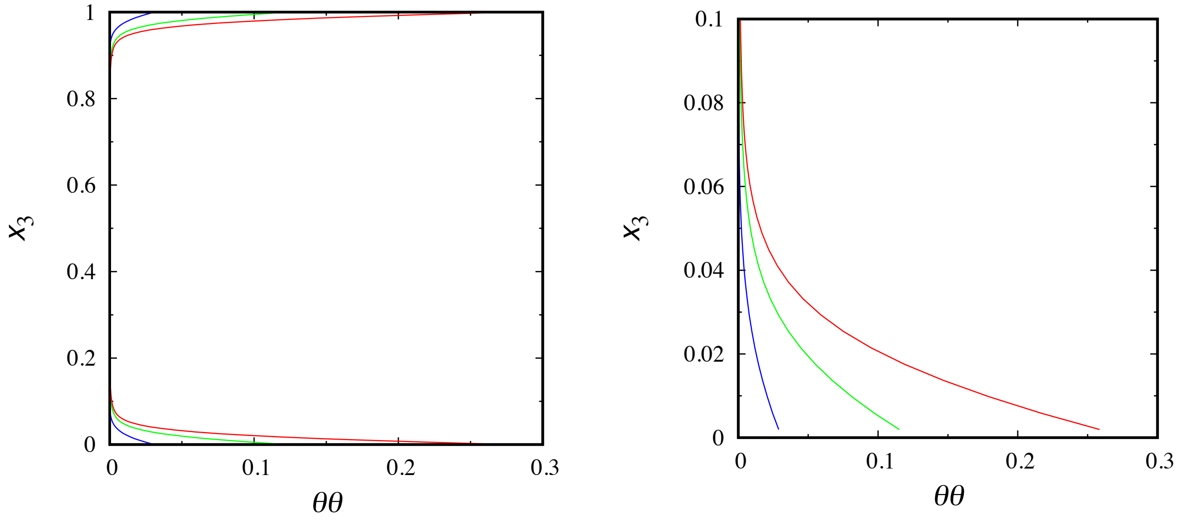

Figure 6: (left) Temperature variance from simulations HET025 (blue), HET050 (green), and HET075 (red). (right) The same as in the left panel but for the lower part of the domain.

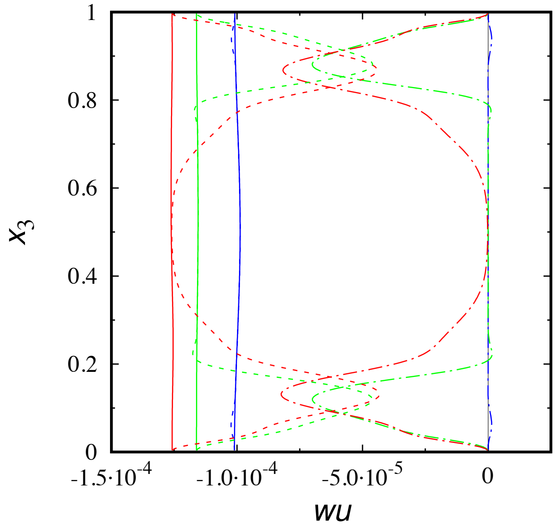

Figure 7: Streamwise momentum-flux component from simulations HET025 (blue), HET050 (green), and HET075 (red). Solid curves show total (turbulent plus molecular) flux, and dot-dashed and dashed curves show contributions due to turbulence and due to molecular diffusion, respectively.

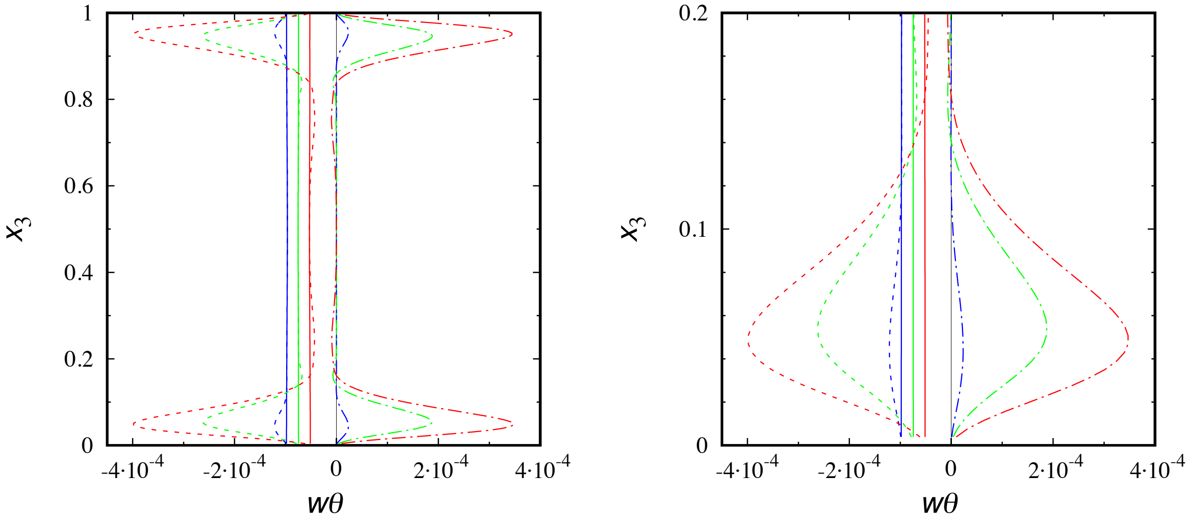

Figure 8: (left) Vertical component of the temperature flux from simulations HET025 (blue), HET050 (green), and HET075 (red). Solid curves show total (turbulent plus molecular) flux, and dot-dashed and dashed curves show contributions due to turbulence and due to molecular diffusion, respectively. (right) The same as in the left panel but for the lower part of the domain.

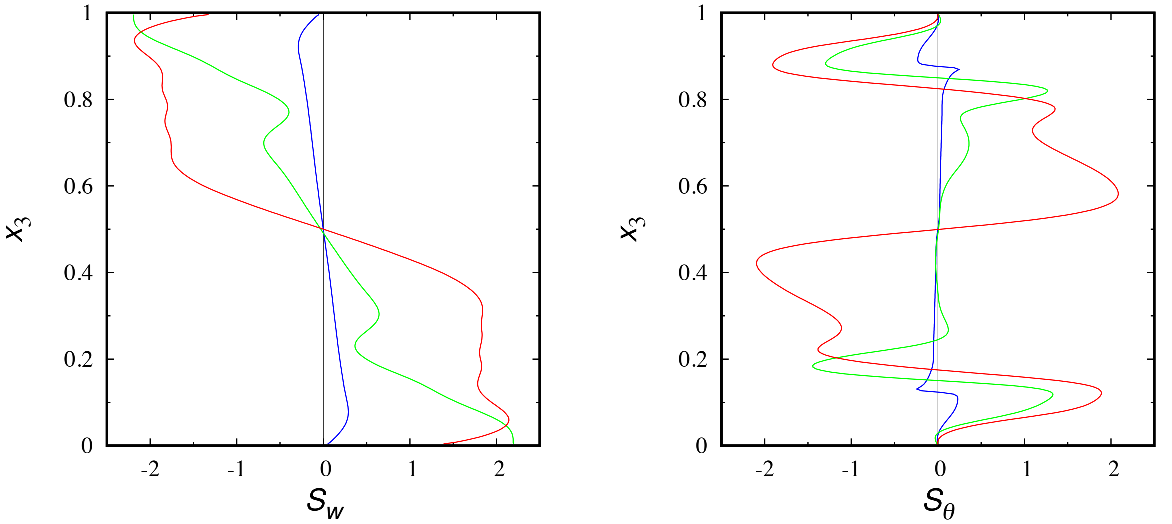

Figure 9: (left) Vertical-velocity skewness and (right) temperature skewness from simulations HET025 (blue), HET050 (green), and HET075 (red).

reveals strongly localized quasi-coherent flow structures characterized by high positive values of the vertical velocity and hight positive fluctuations of potential temperature (about a horizontal-mean temperature). It is these structures that generate positive turbulent potential-temperature flux in the lower part of the flow (Fig. 8), i.e., precisely where both S_w and S_θ are positive (Fig. 9). In the upper part of the flow, large negative vertical velocity (S_w is negative) is collocated with large negative potential-temperature fluctuation (S_θ is negative), leading to a positive turbulent potential-temperature flux.

4.4 FLUX OF TEMPERATURE VARIANCE

Using LES, MS16 performed a comparative analysis of the second-moment budgets and mixing intensity in weakly (moderately) stable boundary layers over thermally-homogeneous and thermally-heterogeneous surfaces. Among other things, the study revealed a key role of the temperature variance in turbulent mixing in a horizontally heterogeneous SBL and an importance of the third-order turbulent transport term in maintaining the temperature-variance budget. Due to the surface heterogeneity, the third-order moment, i.e., the vertical flux of temperature variance (denoted by $w\theta\theta$), is non-zero at the surface. As a result, the turbulent transport term (divergence of the temperature-variance flux) not only redistributes the temperature variance in the vertical, but is a net gain.

The following expression is used to estimate the vertical flux of temperature variance on the basis of LES data:

$$w\theta\theta = \left\langle \overline{\tilde{u}_3'\tilde{\theta}'^2} \right\rangle + \left\langle \overline{\tilde{u}_3'\widetilde{\theta^{s2}}'} \right\rangle + 2\left\langle \overline{\tilde{\theta}'\widetilde{u_3^s\theta^s}'} \right\rangle + \left\langle \overline{\widetilde{u_3^s\theta^{s2}}} \right\rangle , \qquad (12)$$

where a tilde denotes a resolved-scale (filtered) quantity, and the superscript "s" denotes a sub-grid (sub-filter) scale fluctuation. As in the previous sections, an overbar denotes a horizontal-mean quantity, a prime denotes a fluctuation about a horizontal mean, and the angle brackets denote the quantities averaged over time. The first two terms on the r.h.s. of Eq. (12) are zero at the surface because of zero vertical velocity $\tilde{u}_3$. The last term cannot be estimated from the LES but is presumably small (see MS16 and Machulskaya and Mironov, 2018, for discussion). The third term is zero in the homogeneous SBL because of zero $\tilde{\theta}'$ at the surface. In the heterogeneous SBL, surface temperature variations modify local stability conditions and thus modulate the surface temperature flux. The surface temperature $\tilde{\theta}$ and the surface temperature flux $\widetilde{u_3^s\theta^s}$ prove to be positively correlated, leading to a positive flux of temperature variance at the surface.

Within the DNS framework, the expression for the vertical flux of temperature variance reads

$$w\theta\theta = \left\langle \overline{u_3'\theta'^2} \right\rangle - \frac{1}{\mathrm{PrRe}} \frac{\partial \left\langle \overline{\theta'^2} \right\rangle}{\partial x_3} . \qquad (13)$$

It is instructive to establish the correspondence between the LES-based and DNS-based estimates of the temperature-variance flux.

The first two terms on the r.h.s. of Eq. (12) describe the transport of resolved (first term) and sib-grid (second term) temperature variance by the resolved vertical velocity $\tilde{u}_3$. The sum of these terms is in one-to-one correspondence with the first term on the r.h.s. of Eq. (13) that describes the transport of temperature variance by the vertical velocity (there are no sub-grid scale quantities in DNS, hence there is only "total" velocity and "total" temperature variance).

There is no one-to-one matching of the third and the fourth terms on the r.h.s. of Eq. (12) with the second term on the r.h.s. of Eq. (13). It can be readily seen, however, that under certain conditions the LES and DNS terms are closely analogous. If the resolution is sufficiently high, most energy-containing scales of motion are simulated explicitely by the LES code (which is in fact the basic idea of LES), and the sub-grid scale turbulence is nearly isotropic. Then, the sub-grid scale temperature flux is of diffusive and down-gradient character, that is, $\widetilde{u_i^s\theta^s} = -\tilde{\kappa}_s\partial\tilde{\theta}/\partial x_i$, where $\tilde{\kappa}_s$ is the sub-grid scale temperature diffusivity. The third term on the r.h.s. of Eq. (12) becomes

$$2\left\langle \overline{\tilde{\theta}'\widetilde{u_3^s\theta^s}'} \right\rangle = -\left\langle \bar{\tilde{\kappa}}_s \frac{\partial\overline{\tilde{\theta}'^2}}{\partial x_3} \right\rangle - \left\langle \overline{\tilde{\kappa}_s' \frac{\partial\tilde{\theta}'^2}{\partial x_3}} \right\rangle - \left\langle \overline{\tilde{\kappa}_s'\tilde{\theta}'} \frac{\partial\bar{\tilde{\theta}}}{\partial x_3} \right\rangle . \qquad (14)$$

Applying a diffusive down-gradient approximation to the fourth term on the r.h.s. of Eq. (12), we obtain

$$\left\langle \overline{\widetilde{u_3^s\theta^{s2}}} \right\rangle = -\left\langle \bar{\tilde{\kappa}}_s \frac{\partial\overline{\widetilde{\theta^{s2}}}}{\partial x_3} \right\rangle - \left\langle \overline{\tilde{\kappa}_s' \frac{\partial\widetilde{\theta^{s2}}'}{\partial x_3}} \right\rangle . \qquad (15)$$

If the temperature diffusivity $\tilde{\kappa}_s$ does not change considerably in space ($\tilde{\kappa}_s'$ is small) the second and the third terms on the r.h.s. of Eq. (14) and the second term on the r.h.s. of Eq. (15) can be neglected. If changes of $\tilde{\kappa}_s$ in time can also be neglected ($\bar{\tilde{\kappa}}_s - \langle\bar{\tilde{\kappa}}_s\rangle$ is small), then Eqs. (12), (14) and (15) yield the following expression for the LES-based vertical temperature-variance flux:

$$w\theta\theta = \left\langle \overline{\tilde{u}_3'\left(\tilde{\theta}'^2 + \widetilde{\theta^{s2}}'\right)} \right\rangle - \frac{1}{\mathrm{Pr}_s\mathrm{Re}_s} \frac{\partial\left\langle \overline{\tilde{\theta}'^2} + \overline{\widetilde{\theta^{s2}}} \right\rangle}{\partial x_3} . \qquad (16)$$

Here, Pr_s and Re_s and the Prandtl number and the Reynolds number, respectively, defined in terms of (constant) sub-grid scale viscosity and (constant) sub-grid scale temperature diffusivity. Thus, the estimates of the vertical temperature-variance flux based on DNS, Eq. (13), and on LES, Eq. (16), coincide up to definitions of the temperature variance and of the Prandtl and Reynolds numbers.

Vertical profiles of $w\theta\theta$ from our heterogeneous DNS runs are shown in Fig. 10. Both the turbulent contribution and the molecular contribution to $w\theta\theta$ given by the first term and the second term on the r.h.s. of Eq. (13), respectively, are positive close to the lower boundary (by symmetry, these contributions are negative close to the upper boundary). Importantly, the molecular temperature-variance flux is non-zero at the surface. Hence, the third-order transport term not only redistributes the temperature variance in the vertical, but is a net gain. The situation is broadly similar to that in weakly (moderately) stable flows, where the surface thermal heterogeneity produces $w\theta\theta$ that serves to increase the temperature variance in the boundary layer.

5. CONCLUSIONS

Direct numerical simulations at bulk Reynolds number $\mathrm{Re} = 10^4$ and bulk Richardson number $\mathrm{Ri} = 0.25$ are performed to analyze the structure and mixing intensity in strongly stable boundary-layer flows over thermally homogeneous and heterogeneous surfaces. An idealized plane Couette flow set-up is used as a proxy for real-world flows. The flow is driven by a fixed velocity at the upper surface, while the lower surface is at rest. The temperature at the horizontal upper and lower surfaces is either homogeneous or varies sinusoidally in the streamwise direction, while the horizontal-mean temperature is the same in the homogeneous and heterogeneous cases.

The stratification is strong enough to quench turbulence over homogeneous surfaces, resulting in velocity and temperature profiles that vary linearly with height. However, turbulence survives over heterogeneous surfaces. Both the molecular diffusion and the turbulence contribute to the downward, i.e., the down-gradient, transfer of horizontal momentum. The total (diffusive plus turbulent) heat flux is directed downward. However, the turbulent contribution to the heat flux appears to be positive, i.e., up the gradient of the mean temperature. An analysis of the second-order velocity and temperature covariances and of the vertical-velocity and temperature skewness suggests that the counter-gradient heat transport is due to quasi-organized cell-like vortex motions generated by the surface thermal heterogeneity. These motions act to transfer heat upwards similar to quasi-organized cell-like structures that transfer heat upwards in convective boundary layers. Thus, the flow over heterogeneous surface features local convective instabilities and upward eddy heat transport, although the overall stratification remains stable and the heat is transported downward in the mean.

Due to the surface thermal heterogeneity, the vertical flux of temperature variance is non-zero at the surface. As a result, the transport term (divergence of the temperature-variance flux) in the temperature-variance budget not only redistributes the temperature variance in the vertical, but is a net gain. The same effect is encountered in weakly (moderately) stable flows over thermally heterogeneous surfaces, where the third-order transport terms serves to increase the temperature variance in the boundary layer.

A subject of our future work is a comprehensive analysis of the second-moment budgets, where the emphasis is on the turbulence anisotropy and the role of pressure-scrambling effects in maintaining the budgets. Efforts will also be made to use the DNS findings to improve parameterizations of strongly stable boundary layers in large-scale atmospheric models.

Acknowledgments. We thank Alberto de Lozar, Evgeni Fedorovich, Ned Patton, and Jeff Weil for useful discussions.

REFERENCES

Avsarkisov, V., S. Hoyas, M. Oberlack, and J. P. García-Galache, 2014: Turbulent plane Couette flow at moderately high Reynolds number, *J. Fluid Mech.*, **751**, R1.

Deusebio, E., C. P. Caulfield, and J. R. Taylor, 2015: The intermittency boundary in stratifid plane Couette flow, *J. Fluid Mech.*, **781**, 298–329.

Komminaho, J., A. Lundbladh, and A. V. Johansson, 1996: Very large structures in plane turbulent Couette flow, *J. Fluid Mech.*, **320**, 259–285.

Machulskaya, E. and D. Mironov, 2018: Boundary conditions for scalar (co)variances over heterogeneous surfaces, *Boundary-Layer Meteorol.*, doi:10.1007/s10546-018-0354-6.

Mahrt, L., 2014: Stably stratified atmospheric boundary layers, *Ann. Rev. Fluid Mech.*, **46**, 23–45.

Mironov, D., E. Heise, E. Kourzeneva, B. Ritter, N. Schneider, and A. Terzhevik, 2010: Implementation of the lake parameterisation scheme FLake into the numerical weather prediction model COSMO, *Boreal Env. Res.*, **15**, 218–230.

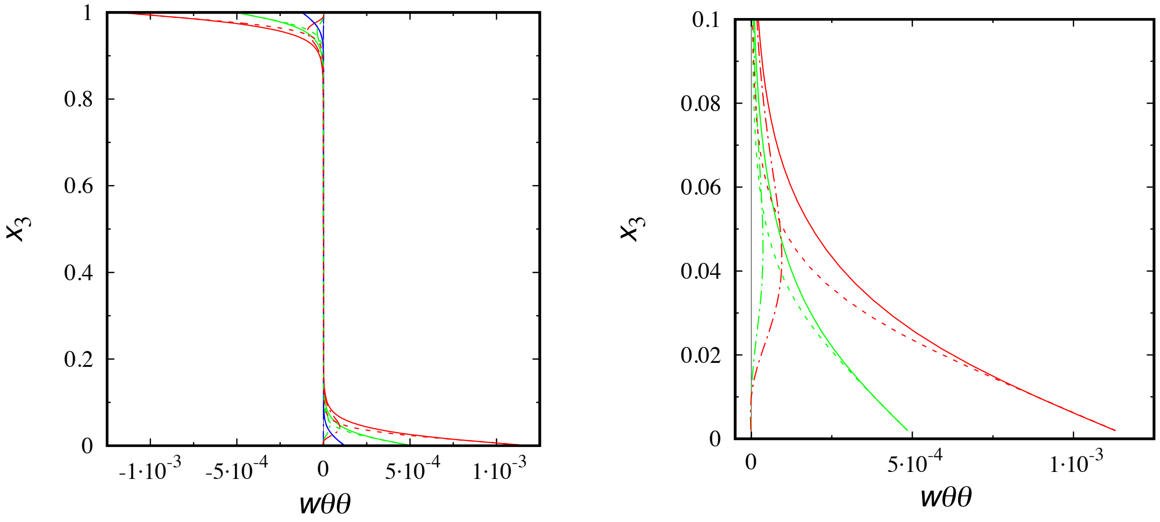

Figure 10: (left) Third-order vertical velocity-temperature covariance (vertical flux of the temperature variance) from simulations HET025 (blue), HET050 (green), and HET075 (red). Solid curves show total (turbulent plus molecular) covariance, and dot-dashed and dashed curves show contributions due to turbulence and due to molecular diffusion, respectively. (right) The same as in the left panel but for the lower part of the domain for simulations HET050 (green) and HET075 (red).

Mironov, D. V. and P. P. Sullivan, 2016: Second-moment budgets and mixing intensity in the stably stratified atmospheric boundary layer over thermally heterogeneous surfaces, *J. Atmos. Sci.*, **73**, 449–464.

Papavassiliou, D. V. and T. J. Hanratty, 1997: Interpretation of large-scale structures observed in a turbulent plane Couette flow, *Int. J. Heat and Fluid Flow*, **18**, 55–69.

Richter, D. H. and P. P. Sullivan, 2014: Modification of near-wall coherent structures by inertial particles, *Phys. Fluids*, **26**, 103304.

Sullivan, P. P. and J. C. McWilliams, 2002: Turbulent flow over water waves in the presence of stratification, *Phys. Fluids*, **14**, 1182–1195.

Sullivan, P. P., J. C. McWilliams, and C.-H. Moeng, 2000: Simulation of turbulent flow over idealized water waves, *J. Fluid Mech.*, **404**, 47–85.